Inorganic Chemistry

ARTICLE

pubs.acs.org/IC

Ferrocenyl Functionalized Silver-Chalcogenide Nanoclusters

Daniel G. MacDonald,[†] Christian Kübel,[‡,§] and John F. Corrigan*[,†]

[†]Department of Chemistry, The University of Western Ontario, London, Ontario, N6A 5B7 Canada

[‡]Institute of Nanotechnology, Karlsruhe Institute of Technology, Hermann-von-Helmholtz-Platz 1, 76344 Eggenstein-Leopoldshafen, Germany

[§]Karlsruhe Nano Micro Facility, Karlsruhe Institute of Technology, Hermann-von-Helmholtz-Platz 1, 76344 Eggenstein-Leopoldshafen, Germany

Supporting Information

ABSTRACT: New (chalcogenoethyl)ferrocenylcarboxalate functionalized silver chalcogenide nanoclusters were synthesized using a combination of silylated chalcogen reagents at low temperatures. The addition of $E(SiMe_3)_2$ to reaction mixtures of $FcC\{O\}OCH_2CH_2ESiMe_3$ (E = S, Se) and $(Ph_3P)_2\cdot AgOAc$ affords nanoclusters with approximate molecular formulas $[Ag_{36}S_9(SCH_2CH_2O\{O\}CFc)_{18}(PPh_3)_3]$ (**1**), $[Ag_{100}Se_{17}(SeCH_2CH_2O\{O\}CFc)_{66}(PPh_3)_{10}]$ (**2**), and $[Ag_{180}Se_{54}(SeCH_2CH_2O\{O\}CFc)_{72}(PPh_3)_{14}]$ (**3**) as noncrystalline solids. Compositions were formulated on the basis of elemental analysis, high resolution transmission electron microscopy, and dynamic light scattering experiments. Solutions of these polyferrocenyl assemblies display a single quasi-reversible redox wave with some adsorption to the electrode surface as studied by cyclic voltammetry. With the smaller clusters **1**, the addition of $[Bu_4N][HSO_4]$ results in a shift of the reduction wave to less positive potentials than those of the complex in the absence of these oxoanions. No further shift is observed after the addition of approximately 1 equivalent of HSO_4^-/ferrocene branch. Cyclic voltammograms of the larger clusters **2** and **3** show the appearance of a new, irreversible wave at less positive potentials than the initial wave upon the addition of HSO_4^-. The appearance of this new wave together with the disappearance of the reduction wave indicates a stronger interaction between the nanoclusters and the hydrogen sulfate anion.

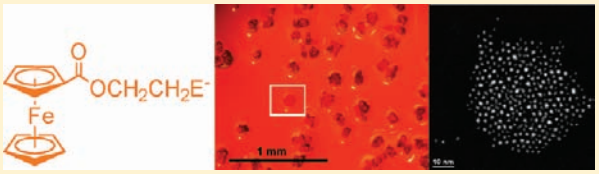

INTRODUCTION

Substantial growth in the development of synthetic approaches and the characterization of d^{10} coinage metal (Cu^I, Ag^I, Au^I) chalcogenide (S, Se, Te) complexes has provided several routes for obtaining highly monodisperse nanometer-sized clusters.[1,2] An efficient method for the introduction of chalcogen into semiconductor metal−chalcogenide nanoclusters is the use of silylated reagents.[2] These reagents have been shown to offer a controlled route to the formation of structurally characterized metal−chalcogenolate/chalcogenide clusters and nanoparticles that are highly monodisperse in nature.[2] They react readily with metal salts via the formation of $XSiMe_3$ (X = Cl, OAc) to yield metal−chalcogenolate (M−ER) and chalcogenide (M−E) bonds (E = S, Se, Te). Notably, the soluble $XSiMe_3$ does not impede the formation and crystallization of the nanometer-sized cluster complexes. Importantly, the tunability of the "R" substituent of $RESiMe_3$ presents the opportunity to control the characteristics of the surface ligands and allow the incorporation of redox active ferrocenyl units onto the core. Our previous works have detailed the functionalization of metal−chalcogen surfaces utilizing the reagents $fc(SeSiMe_3)_2$ and $FcSeSiMe_3$ (fc = $Fe(\eta^5\text{-}C_5H_4)_2$ and Fc = $CpFe(\eta^5\text{-}C_5H_4)$) to introduce $(fcSe)_2^{2-}$ and $FcSe^-$ molecules, respectively, onto the cluster surface.[3,4] Electrochemical measurements (cyclic voltammetry) indicated, however, that cluster decomposition occurs upon oxidation of the Fe(II) centers via the formation of Se−Se bonds.[4] The ferrocenylmethylthiolate nanocluster $[Ag_{48}S_6(SCH_2Fc)_{36}]$ does not degrade upon oxidation of the iron(II) centers and illustrates the possibility of forming clusters whose surfaces have a high ferrocene coverage.[5] The chemistry of high nuclearity silver−chalcogen clusters has been burgeoned recently,[2] although few examples exist which contain ferrocene ligands.[3,6]

Herein, we demonstrate the facile and high yield synthesis and characterization of functionalized silver−chalcogenide nanocluster materials. We describe how the combination of the reagents $FcC\{O\}OCH_2CH_2ESiMe_3$ and $E(SiMe_3)_2$ (E = S, Se) can be used to promote the formation of nanometer-sized particles with ferrocene-rich surfaces. This methodology offers relatively simple handling procedures while providing good control for the preparation of monodisperse clusters. Energy dispersive X-ray analysis (EDX), elemental analysis, UV−visible absorption spectroscopy, transmission electron microscopy (TEM) analysis, NMR spectroscopy, and dynamic light scattering (DLS) have been used to characterize the functionalized silver−chalcogenide nanoclusters **1**−**3**. We also investigate the application of these nanoparticles as HSO_4^- sensors using cyclic voltammetry.

Received: August 24, 2010
Published: March 16, 2011

EXPERIMENTAL SECTION

Materials. All syntheses were performed under an inert atmosphere using standard Schlenk-line techniques or a nitrogen-filled glovebox unless otherwise stated. Tetrahydrofuran, diethyl ether, hexane, and pentane (Caledon HPLC grade) were dried by passing them through packed columns of activated alumina using a commercially available MBraun MB-SP Series solvent purification system. Dichloromethane and chloroform, purchased from Caledon, were distilled over P_2O_5. Starting reagents $E(SiMe_3)_2$ [7] (E = S, Se) were prepared and purified according to literature procedures. The reagents $FcC\{O\}OCH_2CH_2ESiMe_3$ (E = S, Se) were prepared as reported elsewhere.[8] AgOAc was purchased from Strem Chemicals. PPh_3 was purchased from Aldrich Chemicals and used without further purification.

Characterization. ^{1}H NMR spectra were obtained on a Varian INOVA 400 MHz spectrometer at an operating frequency of 399.76 MHz and are reported in parts per million. ^{1}H NMR spectra were referenced internally to residual H of the deuterated solvent relative to tetramethylsilane ($SiMe_4$) at 0 ppm. Ultraviolet−visible spectra were recorded on a Varian Cary 300 Bio UV−vis spectrophotometer in CH_2Cl_2. Elemental analyses were performed by Guelph Chemical Laboratories (Guelph, Canada) and Columbia Analytical Services (Tucson, AZ). Energy dispersive X-ray (EDX) analyses of thermolyzed material were performed at Surface Science Western (UWO). A Quartz Xone EDX analysis system coupled to a Leo 440 SEM equipped with a Gresham light element detector was used to obtain semiquantitative analysis of Ag, S, Se, and Fe. Analyses were carried out using a 20 kV electron beam rastered over a 100 μm × 100 μm area and were repeated to ensure reproducibility.

Transmission electron microscopy (TEM) analyses were performed at the Institute of Nanotechnology, Karlsruhe Institute of Technology, Germany using an image corrected FEI Titan 80−300 electron microscope operating at 300 kV. TEM samples were prepared by dropping dilute THF solutions of the nanoclusters onto carbon coated Cu-plated grids (Quantifoil holey carbon grids coated with 2 nm carbon), and excess solvent was allowed to evaporate. The TEM was equipped with an EDAX sUTW Energy-Dispersive X-ray detector. The analyses were carried out in the STEM mode with a HAADF (High Angle Annular Dark Field) detector using a nominally 0.15 nm sized probe.

A BAS 100 electrochemical workstation using a three-electrode system, with a platinum working electrode, a platinum flag counter electrode, and a saturated Ag/AgCl reference electrode with 0.1 M $[NBu_4][PF_6]$ in CH_2Cl_2 as the supporting electrolyte was used for electrochemical measurements. The potentials are reported versus saturated Ag/AgCl.[9] Molecular formulas were estimated as described in the Results and Discussion. Concentrations of solutions calculated by using formulas of $[Ag_{36}S_9(SCH_2CH_2O\{O\}CFc)_{18}(PPh_3)_3]$, $[Ag_{100}Se_{17}(SeCH_2CH_2O\{O\}CFc)_{66}(PPh_3)_{10}]$, and $[Ag_{180}Se_{54}(SeCH_2CH_2O\{O\}CFc)_{72}(PPh_3)_{14}]$ for **1**, **2**, and **3**, respectively, were used. Some uncertainty is associated with these calculated formulas, as these were adjusted slightly from the elemental composition to satisfy charge balance. The electrolyte $[Bu_4N][PF_6]$ was placed in the electrochemical cell containing the working, counter, and reference electrodes. Dichloromethane (DCM) was then added and the system degassed with N_2. A blank voltammogram was recorded without the particles to check the working electrode. The particles (10 mg) were then solubilized in a minimum amount of DCM and added to the cell. The solution was stirred and degassed; then a cyclic voltammogram (CV) was recorded. Oxoanions were then added in small quantities using a pipet. After each addition, the solution was degassed and a CV recorded.

Synthesis. *Synthesis of* ***1***. AgOAc (1.10 mmol) was dissolved in 10 mL of $CHCl_3$ with the addition of PPh_3 (2.20 mmol). $FcC\{O\}OCH_2CH_2SSiMe_3$ (0.83 mmol) in 5 mL of $CHCl_3$ was added to this clear colorless solution at −50 °C followed immediately by $S(SiMe_3)_2$ (0.14 mmol). The reaction was warmed to room temperature slowly with stirring and was stirred for a further 2 h at RT yielding a red solution. The stirbar was then removed, and the red solution was layered with 15 mL of cyclohexane. After a few days, 0.26 g of **1** was obtained as red−orange blocks. ^{1}H NMR (400 MHz, $CDCl_3$, δ): 7.38−7.34 (bm, Ph, 2.3 H), 4.77 (bs, CH, 2.0 H), 4.52 (bs, CH_2, 2H), 4.21 (s, CH, 2H), 4.11 (s, Cp, 5H), 3.37 (bs, CH_2, 2H). Anal. (%) found for **1**: C, 32.92; H, 2.81; O, 4.42; P, 1.6; Fe, 9.93; S, 8.93; Ag, 36.78. Anal. (%) calcd for $[Ag_{36}S_9(SCH_2CH_2O\{O\}CFc)_{18}(PPh_3)_3]$: C, 34.0; H, 2.8; O, 5.7; P, 0.9; Fe, 9.9; S, 8.5; Ag, 38.2.

Synthesis of ***2***. AgOAc (0.82 mmol) was dissolved in 10 mL of $CHCl_3$ with the addition of PPh_3 (1.63 mmol). A solution of $FcC\{O\}OCH_2CH_2SeSiMe_3$ (0.61 mmol) in 5 mL of $CHCl_3$ was added to the clear colorless solution at −50 °C followed by $Se(SiMe_3)_2$ (0.10 mmol). The reaction was allowed to warm to room temperature slowly with stirring and was stirred for a further 2 h at RT, with the color changing from clear orange to blood red. The stir bar was then removed, and the dark red solution was layered with 15 mL of hexane. After a few days, 0.16 g of **2** was obtained as dark red blocks. ^{1}H NMR (400 MHz, $CDCl_3$, δ): 7.44−7.35 (bm, Ph, 2.2 H), 4.78 (s, CH, 2H), 4.53 (bs, CH_2, 2 H), 4.23 (s, CH, 2H), 4.13 (s, Cp, 5H), 3.33. (bs, CH_2, 2H). Anal. (%) found for **2**: C, 32.74; H, 3.05; O, 5.53; P, 0.60; Fe, 8.7; Se, 17.4; Ag, 29.8. Anal. (%) calcd for $[Ag_{100}Se_{17}(SeCH_2CH_2O\{O\}CFc)_{66}(PPh_3)_{10}]$: C, 33.8; H, 2.8; O, 5.7; P, 0.8; Fe, 10.0; Se, 17.8; Ag, 29.2.

Synthesis of ***3***. AgOAc (1.22 mmol) was dissolved in 10 mL of $CHCl_3$ with the addition of PPh_3 (2.44 mmol). A solution of $FcC\{O\}OCH_2CH_2SeSiMe_3$ (0.61 mmol) in 5 mL of $CHCl_3$ was added to the clear colorless solution at −50 °C followed by $Se(SiMe_3)_2$ (0.31 mmol). The reaction was warmed to room temperature slowly with stirring and was stirred for a further 2 h at RT, yielding a brown-red solution upon stirring overnight. The stir bar was then removed, and the dark solution was layered with 15 mL of hexane. After a few days, 0.16 g of **3** was obtained as black blocks. ^{1}H NMR (400 MHz, $CDCl_3$, δ): 7.46−7.38 (bm, Ph, 2.9H), 4.77 (s, CH, 2H), 4.49 (bs, CH_2, 2H), 4.23 (s, CH, 2H), 4.11 (s, Cp, 5H), 3.27. (bs, CH_2, 2H). Anal. (%) found for **3**: C, 29.54; H, 2.12; O, 3.94; P < 0.80; Fe, 7.68; Se, 17.3; Ag, 37.07. Anal. (%) calcd for $[Ag_{180}Se_{54}(SeCH_2CH_2O\{O\}CFc)_{72}(PPh_3)_{14}]$: C, 27.7; H, 2.2; O, 4.5; P, 0.8; Fe, 7.8; Se, 19.3; Ag, 37.7.

RESULTS AND DISCUSSION

Synthesis. There are several routes documented for the synthesis of metal chalcogen nanocluster complexes.[2a,10] One of the most versatile methods involves the use of silylated chalcogen reagents such as $E(SiMe_3)_2$ and $RESiMe_3$ (R = alkyl, aryl, Fc; E = S, Se, Te). The generality of this approach is demonstrated by the ability of these main group complexes to react with a wide range of metal salts including those of early and late transition and main group metals.[2a] Furthermore, this route offers access to a wide range of cluster complexes from the truly molecular to structurally characterized nanoclusters such as $[Cu_{146}Se_{73}(PPh_3)_{30}]$[11] and $[Ag_{490}S_{188}(StC_5H_{11})_{114}]$[1g] that can be viewed as nanometer-sized cutouts of the bulk semiconductor materials. Importantly, this synthetic methodology permits the incorporation of surface functionalities onto the semiconductor core, which can modulate or alter the properties of the cluster frameworks.[12] Our approach to ferrocenyl functionalized complexes involves a development of this method via the synthesis of suitable ferrocene-containing ligands with reactive trimethylsilylchalcogenide functionalities.[3,4,6] In this manner, the nanoscopic cluster $[Ag_{48}S_6(SCH_2Fc)_{36}]$ has been prepared and structurally characterized via a single crystal diffraction analysis.[5]

dx.doi.org/10.1021/ic101717z |*Inorg. Chem.* 2011, 50, 3252–3261

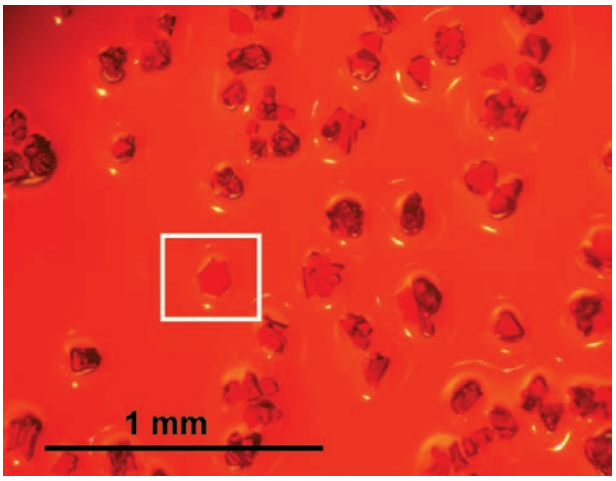

Figure 1. Isolated samples of **1**. The square box highlights what appears to be a single crystal.

When a freshly prepared solution of $FcC\{O\}OCH_2CH_2SSiMe_3$[8] was reacted with $(Ph_3P)_2\cdot AgOAc$ together with $S(SiMe_3)_2$ at −50 °C in $CHCl_3$, followed by slow warming to room temperature, a deep red solution was obtained. Layering of the reaction mixture with cyclohexane resulted in the formation of orange, plate-like crystals of **1**. The reaction yields what appear to be single crystals, as illustrated in Figure 1 for **1**. However, despite numerous attempts from repeat reactions and crystallizations, no well-defined, sharp single crystal or powder X-ray diffraction pattern was observed in the 2θ range of 5 to 105°. There was no evidence of desolvation during these analyses, which could account for the lack of crystallinity, suggesting a general lack of long-range order within the solid. The analogous silver selenide particles **2** were synthesized in a similar manner to **1** (eq 1) by the reaction of PPh_3 solubilized AgOAc with a combination of bis(trimethylsilyl)selenide and $FcC\{O\}OCH_2CH_2SeSiMe_3$.[8] These clusters can also be isolated from the reaction solution upon layering with hexane or cyclohexane as small deep red blocks after several days at room temperature. As was observed for **1**, no well-defined, sharp X-ray diffraction pattern was observed for **2**, indicating the same lack of long-range order within what appear to be single crystals. This lack of crystallinity in otherwise monodisperse nanoclusters (see below) may be a reflection of the structurally flexible $FcC\{O\}OCH_2CH_2-$ chains that passivate the surfaces, although Hopper growth and contact twinning were also a commonly observed problem during attempted crystallization of clusters **1** and **2**. Particles **1** and **2** are stable for extended periods at ambient conditions in the solid state in the presence of both oxygen and moisture.

$$4AgOAc + 8PPh_3 + 3FcC\{O\}OCH_2CH_2ESiMe_3 + 0.5\ E(SiMe_3)_2 \rightarrow \mathbf{1}\ \text{and}\ \mathbf{2}\ \mathbf{1}, E = S; \mathbf{2}, E = Se \quad (1)$$

Control over the amount of interstitial chalcogenide incorporated (i.e., from $E(SiMe_3)_2$) in these reactions presents an opportunity for modifying the size of the cluster/particle as E^{2-} tends to form interstitial M−E (M = metal) bridging interactions with higher coordination numbers than M−ER and can ultimately result in larger cluster frameworks.[2] Larger ratios of E^{2-} to metal in the reactions generally result in the formation of larger, more condensed frameworks. The generality of this approach has given rise to a wide range of metal chalcogen clusters with varying core sizes depending on the ratio of metal/chalcogenide/chalcogenolate utilized.[2d] In this vein, particles of **3** were prepared in a similar manner to **2** but with a larger $Se(SiMe_3)_2$ to AgOAc ratio in order to increase the quantity of interstitial selenide incorporated into the framework.

The addition of a freshly prepared solution of $FcC\{O\}OCH_2CH_2SeSiMe_3$ to AgOAc solubilized with PPh_3 followed by $Se(SiMe_3)_2$ at −50 °C in $CHCl_3$ (eq 2) yields an almost black solution upon subsequent warming to room temperature. Layering of the reaction mixtures with hexane results in the formation of crystal-like solids of **3** as black blocks. The crystals of **3** show no decomposition in air and are remarkably stable in solution (NMR, ECHEM) under an inert atmosphere. As observed with the smaller particles **1** and **2**, the well-defined solid (shape, edges, size) **3** also does not display any well-defined diffraction pattern when analyzed using X-ray crystallographic techniques. This is in agreement with TEM observations, which, despite confirming a rather monodisperse size distribution of nanoclusters, also reveal aggregated supramolecular crystals with a diameter in the range of only 20−50 nm (*vide infra*).

$$2AgOAc + 4PPh_3 + 1FcC\{O\}OCH_2CH_2SeSiMe_3 + 0.5\ Se(SiMe_3)_2 \rightarrow \mathbf{3} \quad (2)$$

During the formation of nanoclusters **1**−**3**, sharp color changes are observed with increasing temperature. As the temperature slowly climbs from −50 °C, the clear solutions generally remain light orange in color (the orange color stemming from the presence of the ferrocenyl moieties). However, from approximately −10 to 0 °C, the reaction mixtures begin to darken and slowly become a bright red color around 10 °C. The final color changes occur while the solutions are stirred at room temperature for several hours. The red color darkens to a deep opaque blood red color for the smaller particles, while reactions yielding the larger particles proceed to give an almost black reaction solution.

Similar reactions with other tertiary phosphines (i.e., PPr_3, $P(p\text{-}CH_3C_6H_5)_3$, $PEtPh_2$) were performed to probe the effect, if any, of differing R substituents on the crystallinity of the particles. The reactions, however, typically yielded solids with less defined features (less "crystal like"). Phosphine exchange reactions were also attempted where solutions of isolated **1**−**3** were mixed with tri-*p*-tolylphosphine (as it has a similar cone angle to that of PPh_3). Crystalline material similar to that observed previously for **1**−**3** was obtained; again, however, no well-defined diffraction was observed with the isolated samples either. The synthetic conditions were manipulated such that different solvents, different ratios of solvents, and different crystallization temperatures were used in attempts to promote crystallization, all of which at this time have failed to yield materials in the form of single crystals.

NMR Spectroscopy. For **1**, it was found that there is an upfield shift in the ^1H NMR spectra for the protons associated with the ferrocenyl moiety (4.77, 4.21, 4.11 ppm) versus the uncoordinated reagent $FcC\{O\}OCH_2CH_2SSiMe_3$ (4.81, 4.39, 4.21 ppm). A distinct downfield shift of the protons associated with the methylene bridge ($FcC\{O\}O-\mathbf{CH_2CH_2}-S$) (4.52, 3.37 ppm) was also observed (4.29, 2.79 pm; $FcC\{O\}OCH_2CH_2SSiMe_3$; peaks d and e in Figure 2). Reactions of the selenium reagent $FcC\{O\}OCH_2CH_2SeSiMe_3$ with $(Ph_3P)_2\cdot AgOAc$ are consistent, according to the ^1H NMR spectra, with those observed for reactions with the sulfur-based reagents.

dx.doi.org/10.1021/ic101717z |*Inorg. Chem.* 2011, 50, 3252–3261

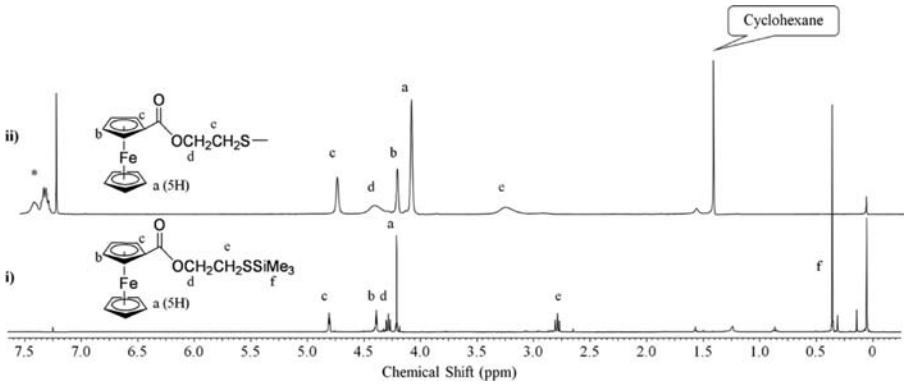

Figure 2. ^{1}H NMR spectra of (i) reagent FcC{O}$OCH_2CH_2SSiMe_3$ and (ii) **1** obtained in $CDCl_3$. The ∗ indicates protons of PPh_3 ligands.

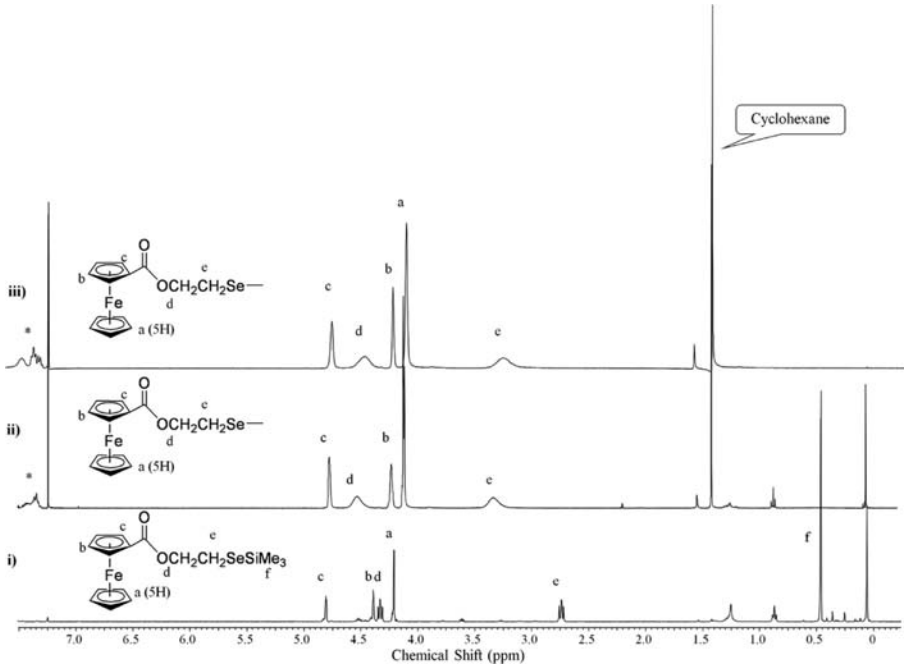

Figure 3. ^{1}H NMR of (i) reagent FcC{O}$OCH_2CH_2SeSiMe_3$, (ii) **2**, and (iii) **3** obtained in $CDCl_3$. The ∗ indicates PPh_3 protons.

The spectra of the particles (Figure 3) clearly display the five characteristic selenolate ligand (FcC{O}$OCH_2CH_2Se^-$) signals, in addition to the signals of coordinated triphenylphosphine ligands. The chemical shifts of the ferrocenyl protons are almost identical to those of the analogous sulfide particles; however, a slight shift is observed in the peaks associated with the two methylene protons of the ligands of the silver−selenide particles (**2** and **3**).

The similarity of the ferrocenyl proton signals for all particles is expected, as the environment about the organometallic moiety does not change substantially with increasing particle size. This is further confirmed upon comparison of the ferrocenyl proton signals of **1** with those of the structurally characterized cluster $[Ag_{14}S(SCH_2CH_2O\{O\}CFc)_{12}(PPh_3)_6]$.[8] The signals of the ferrocenyl protons have almost identical chemical shifts (4.77, 4.21, 4.11 ppm, **1**; 4.76, 4.29, 4.12 ppm, $[Ag_{14}S(SCH_2CH_2O\{O\}CFc)_{12}(PPh_3)_6]$) although a larger difference in the chemical shifts of the methylene proton peak signals is observed ($\Delta\delta$ = 0.33 ppm). Additionally, a distinct broadening of the signals can be observed upon coordination of the ligands to the large silver−chalcogenide frameworks in **1**−**3**, consistent with anchoring of the ligands to larger particles.[13] The clusters appear, via NMR spectroscopy, to be stable in solution.

The presence of free triphenylphosphine in the ^{1}H NMR spectra of the resultant reaction solutions indicates that a large portion of these monodentate ligands is displaced from the silver center upon coordination of the chalcogenolate ligands. The triphenylphosphine ligands, being rather labile, are easily displaced by the chalcogen via bridging interactions between silver. The spectra of **1**−**3** exhibit peaks corresponding to coordinated triphenylphosphine as well as peaks associated with the protons of the ferrocene-containing ligands. An approximate ferrocene/phosphine ratio can be calculated via integration of the respective proton signals, giving a ratio of ∼6:1 for **1**, ∼7:1 for **2**, and ∼5:1 for **3**.

Nanocluster Characterization. Due to the inability to obtain the structural composition of the nanoclusters via single crystal and powder X-ray diffraction techniques, several other analytical techniques were employed to determine a molecular composition including thermogravimetric analysis (TGA), transmission

dx.doi.org/10.1021/ic101717z |*Inorg. Chem.* 2011, 50, 3252–3261

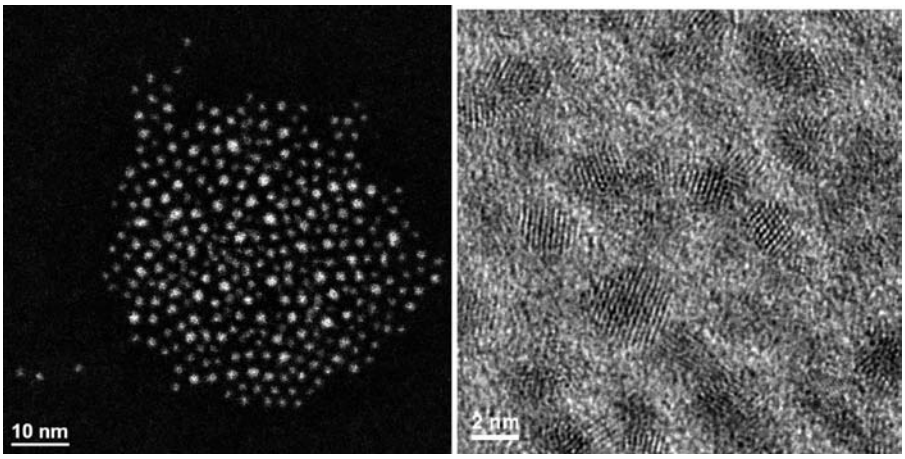

Figure 4. (S)TEM imaging of **1**. (a) HAADF-STEM image (median filtered) of **1**. (b) Aberration corrected HRTEM image of Ag nanoparticles (exhibiting lattice fringes with 0.238 nm distance) formed by electron beam decomposition of **1**.

electron microscopy (TEM), dynamic light scattering (DLS), and elemental analysis (EA).

Thermogravimetric Analysis. The average ligand count of ferrocenated alkanethiolate stabilized gold nanoparticles is often determined using thermogravimetric analysis (TGA). In most cases, for thiolate stabilized gold nanoparticles, the organic fraction is eliminated as the corresponding disulfide, leaving behind elemental gold.[14] This process has also been used in the analysis and preparation of metal−chalcogen nanoparticle materials; however the surface chalcogenolates are eliminated as monochalcogenides (RER; E = S, Se; R = any organic group).[15] The nanoclusters **1** and **3** were heated gradually (10 °C/min) from room temperature 25° to 550 °C under nitrogen, shown in Figures S1 and S2 for particles **1** and **3**, respectively (Supporting Information). Instead of the step-like mass loss typically observed when thiolate ligands of ferrocenylalkylthiolate functionalized gold nanoparticles are thermolyzed,[16] the mass loss occurred as a multistep process. These multiple steps arise from the presence of different ligands (PPh_3, $FcC\{O\}OCH_2CH_2S^-$) on the surface together with some cyclohexane of crystallization, as indicated by ^1H NMR spectroscopy, each of which likely undergo thermally induced elimination at different temperatures. The total mass loss observed was ∼38% for **1** and ∼33% for **3**. Upon inspection of the alumina crucible, a significant amount of a rust colored material remained. EDX analysis of this material indicated that silver, sulfur, and iron were present in a ratio of 1:1:0.5 for **1**. If $FcC\{O\}OCH_2CH_2S^-$ was eliminated completely as $(FcC\{O\}OCH_2CH_2)_2S$, no iron would be expected to remain in the sample. Analysis of the volatile products from the TGA by ^1H NMR spectroscopy reveals that they are comprised of PPh_3 and FcCOOH. The presence of ferrocencarboxylic acid in the volatile components suggests that the decomposition is occurring, at least partially, through cleavage about the ester of the ligands, yielding $FcCOO^-$. As a result, TGA data were inconclusive and could not be further used in the determination of the molecular formula. The results of the elemental analysis for the particles are summarized in the Experimental Section. When atomic percentages (obtained from the weight percent) were used, an overall ratio of the elements present was determined, which was used in conjunction with the HRTEM (below) data to derive the formulas for **1**−**3**.

Electron Microscopy. The particles were characterized using high resolution−transmission electron microscopy (HR-TEM) and scanning transmission electron microscopy (STEM) in order to determine particle core size. It is clear from the images, illustrated in Figures 4 (**1**) and 5 (**3**), that discrete, well-defined particles have been prepared. The particles appear to be spherical in nature, which is a common feature of larger Ag_2S nanoclusters.[1g] Some larger particles can be observed in the TEM images about the center of the sample. In the case of **1**, only isolated, randomly arranged nanoparticles are observed by STEM, whereas also some small superlattice crystals are observed for **3**, which are formed by cubic packing of the individual nanoclusters (Figure 6). The core diameters of **1** (Figure 4a) and **3** (Figure 5a) have been determined from the HAADF-STEM images to have an average diameter of ∼1.3 ± 0.2 nm and 2.3 ± 0.3 nm, respectively. This measurement might be slightly affected by the ferrocene ligands, but the increased particle size of **3** versus **1** is consistent with the reaction scheme used (eq 2), as the larger framework is related to the incorporation of more interstitial chalcogenide. Quantitative EDX analysis of these nanoclusters indicate approximate ratios of 36Ag/35S/21Fe/3P and 180Ag/119Se/78Fe/4P for **1** and **3**, respectively, consistent with the molecular formulas derived. The nanoparticles are fairly sensitive to electron beam exposure and under semi low-dose operation conditions for HRTEM only crystalline particles are observed, whose lattice spacings match those of crystalline silver (Figures 4b and 5b). This is due to electron beam induced reduction of the silver−chalcogen particles.

DLS Analysis. A DLS analysis of solutions of **1** indicated an overall hydrodynamic diameter of ∼3.3 nm for the particles with a polydispersity of 0.07, which indicated very little aggregation. This size is consistent with the core size (1.3 nm) observed from the STEM images above. As the ligand $FcC\{O\}OCH_2CH_2S$ is approximately 0.88 nm in length (based on distances calculated from the crystal structure of $[Ag_{14}S(SCH_2CH_2O\{O\}CFc)_{12}(PPh_3)_6]$),[8] a spherical particle core diameter of 1.3 nm with a surface functionalized by $FcC\{O\}OCH_2CH_2S$ would yield particles ∼3.0 nm (1.3 + (2 × 0.88)) in diameter, consistent with the particle diameter obtained from DLS investigations. DLS analysis of **2** and **3** revealed that these particles had an overall hydrodynamic diameter of ∼6.1 and 6.4 nm, respectively, with very little aggregation, resulting in a low polydispersity of 0.17 and 0.11. For **3**, the diameter of 6.4 nm is larger than the particle diameter calculated from the TEM images (Figure 5; ∼ 2.3 nm) combined with the known length of the FcC

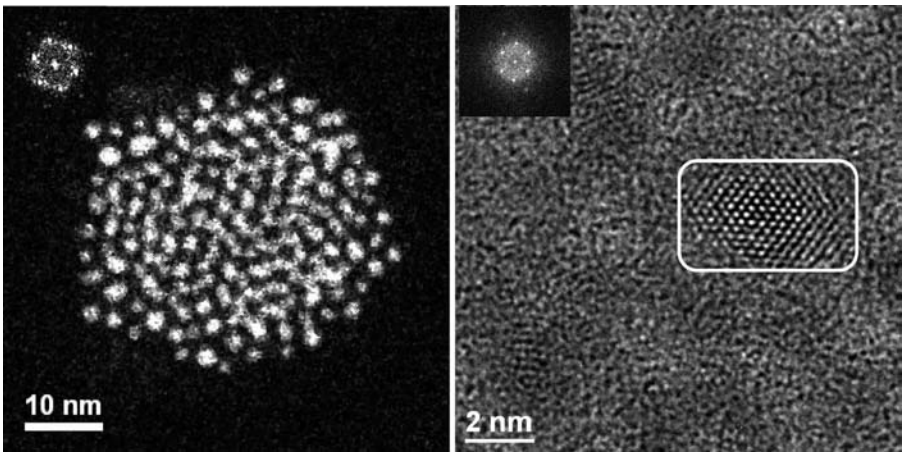

Figure 5. (S)TEM imaging of **3**. (a) HAADF-STEM image (median filtered) and FFT of **3**. The primary particles are arranged in a hexagonal 2D pattern with lattice spacings of 2.7 nm. (b) Aberration corrected HRTEM image of Ag nanoparticles formed by electron beam decomposition of **3**. The box highlights a single Ag particle imaged in ⟨110⟩ zone axis orientation with measured lattice spacings of 0.205, 0.235, and 0.245 nm.

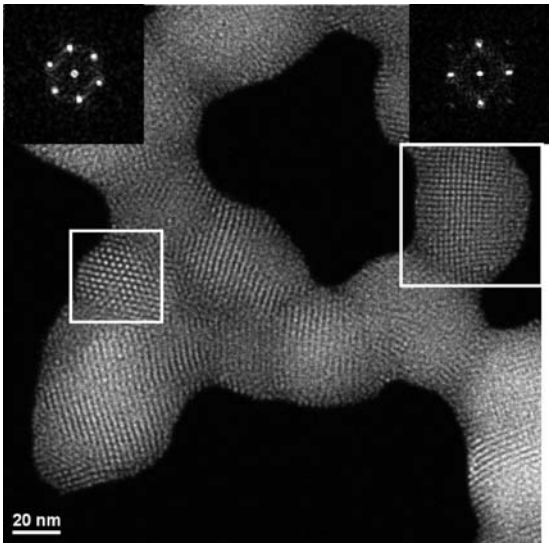

Figure 6. HAADF-STEM image of **3** nanocrystal aggregates. The two selected FFTs fit to the ⟨111⟩ and ⟨100⟩ projection of the cubic packing of nanoclusters with unit cell parameters of 4.5 nm.

$\{O\}OCH_2CH_2Se^-$ (2 × 0.88 nm) ligands. However, it is possible that the particles are not symmetrical in shape, as disk and cylindrical core shapes have been observed for other large silver selenide clusters; although this was not observed in the TEM images.[1] In this context, aggregation of the clusters in solution cannot be discounted.

From these data, a qualitative estimate of the number of silver and sulfur atoms present in the core of **1** can be calculated. As discussed earlier, numerous nanoscopic silver sulfide clusters have been structurally characterized and reported.[1] Thus, a comparison of the core size with the core size of clusters whose structure has been determined can provide a good estimate of the number of atoms within the core. Careful examination of the literature indicated that a core diameter of ∼1.3 nm likely corresponds to approximately 40−50 silver atoms, 5−10 chalcogenide atoms, and 30−40 chalcogenolate ligands,[17] while a core of 2.3 nm relates to approximately 150−200 silver atoms, 40−60 chalcogenide atoms, and 60−80 chalcogenolate ligands.[18] From this information combined with the atomic ratios obtained from the elemental analysis, we can suggest that the molecular formula of **1** lies approximately between $[Ag_{36}S_9(SCH_2CH_2O\{O\}CFc)_{18}(PPh_3)_3]$ and $[Ag_{48}S_{12}(SCH_2CH_2O\{O\}CFc)_{24}(PPh_3)_4]$ and that the molecular formula of **3** lies somewhere between $[Ag_{156}Se_{45}(SeCH_2CH_2O\{O\}CFc)_{66}(PPh_3)_{10}]$ and $[Ag_{204}Se_{58}(SeCH_2CH_2O\{O\}CFc)_{88}(PPh_3)_{16}]$, although a more exact determination is currently not possible in the absence of single crystal X-ray data.

Ultraviolet−Visible Spectroscopy. The solution electronic absorption spectra of **1**−**3** are displayed in Figure 7. An absorption spectrum of $FcC\{O\}OCH_2CH_2Br$[8] has been included for reference as the surface of the particles has been functionalized with $FcC\{O\}OCH_2CH_2E^-$ ligands (E = S, Se). The spectrum of $FcC\{O\}OCH_2CH_2Br$ displays three characteristic maxima: a relatively broad maximum at 311 nm, a shoulder at 345 nm, and a broad absorption maximum at 445 nm. The three absorptions are consistent with those observed for other ferrocenes substituted with carbonyl moieties, such as acetylferrocene,[19] and result from either Fe(II) d−d transitions or a metal−ligand charge transfer (MLCT) process ($d_\pi-\pi^*$) transition. Additionally, a strong absorption is observed at ∼260 nm corresponding to a ligand-centered (Cp rings) $\pi-\pi^*$ transition.

Consistent with the assignment of the spectra of $FcC\{O\}OCH_2CH_2Br$, nanoclusters **1**−**3** display two of the characteristic $FcC\{O\}CH_2CH_2-$ ligand absorption maxima at ∼310 and ∼350 nm. The absorptions appear more as shoulders rather than the discrete maxima observed for $FcC\{O\}OCH_2CH_2Br$. The intense $\pi-\pi^*$ absorption band of the aromatic groups is also observed at ∼260 nm. The d−d transition typically observed at approximately 444 nm in ferrocenyl complexes is not resolved in **1**−**3** due to an intense overlapping absorption arising from the Ag−E framework. The absorption spectra of the related and structurally characterized silver sulfide cluster, $[Ag_{14}S(SCH_2CH_2O\{O\}CFc)_{12}(PPh_3)_6]$,[8] was dominated primarily by the ferrocene and phosphine absorptions. This, however, is not the case observed for the larger silver−sulfide nanocluster **1** (Figure 7) prepared here. The absorption spectra of the particles are instead dominated by an absorption with an onset of ∼460 and 500 nm, respectively. Silver sulfide nanoparticles with an average particle size of 2.3 nm display a similar spectrum with an absorption onset at ∼550 nm.[20] These absorption profiles are typical of silver sulfide (Ag_2S) nanoparticles with the electronic

dx.doi.org/10.1021/ic101717z |*Inorg. Chem.* 2011, 50, 3252–3261

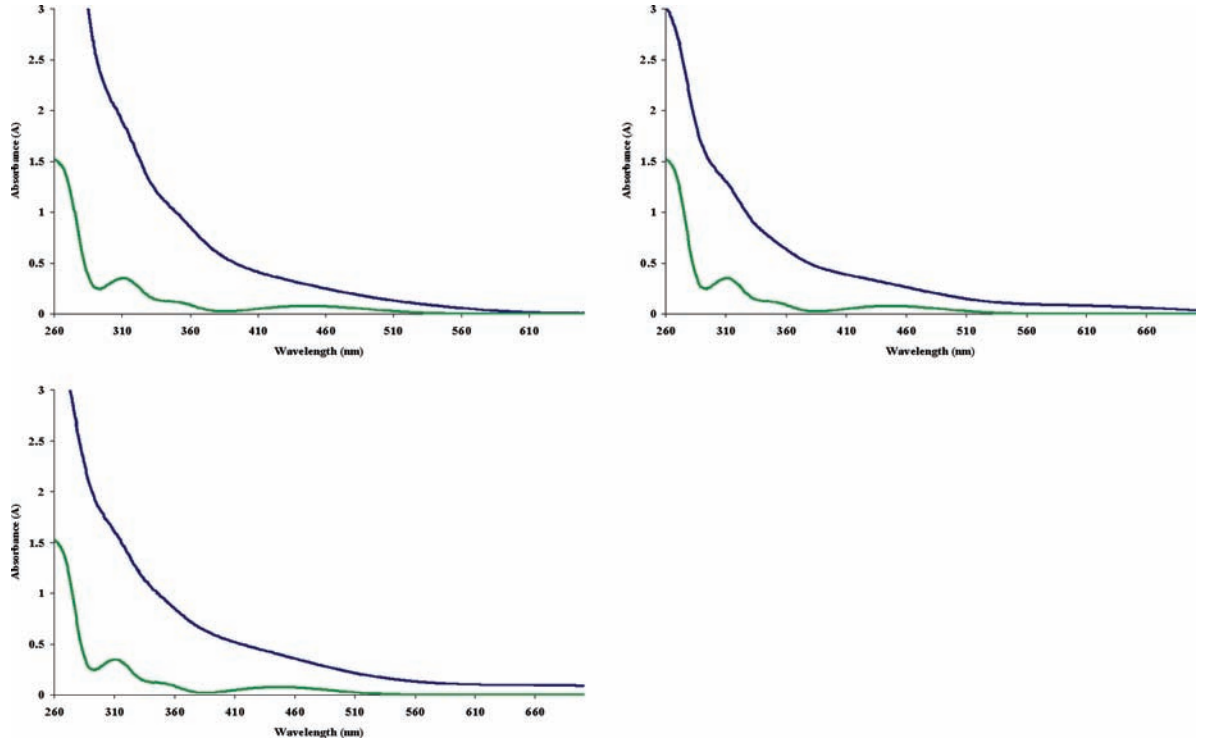

Figure 7. Absorption spectra of **1** (top left), **2** (top right), and **3** (bottom left) at concentrations of (10 mg/10 mL (blue) with FcC{O}CH_2CH_2Br (1.5×10^{-4} M) (green) for comparison.

transition from the valence band to conduction band has been assigned to a 3p(S)→5s(Ag) ligand to metal charge transfer (LMCT).[21] Similarly, the electronic absorption spectra of the analogous silver selenide particles **2** and **3** are dominated by the 4p(Se)→5s(Ag) LMCT; however the absorption onsets are slightly red-shifted compared to those of the silver−sulfide particles at 510 and 560 nm, respectively, and once again the lower energy d−d transition of the ferrocenyl fragment ligand (444 nm) is not resolved.

Cyclic Voltammetry. Cyclic voltammograms of ferrocene display a single oxidation−reduction wave, corresponding to a single electron oxidation (Fe(II) to Fe(III)) per molecule of ferrocene. Similarly, cyclic voltammograms of many multiple ferrocenyl assemblies (ferrocenated nanoparticles, polymers, and dendrimers) often display a single redox wave. In these cases, however, the wave corresponds to the oxidation of all the ferrocenes about the surface of the molecules, which is a multi-electron process. The appearance of a single wave indicates that the electrostatic factor (electrostatic interaction between ferrocenes) is negligible. Bard and co-workers[22] have demonstrated using poly(vinyl)ferrocene that the oxidation potential of each ferrocene is actually statistically distributed along the CV wave. These results suggest that the ferrocenes do not actually oxidize at the same potential, but they are so close that the CV wave can be considered as a single wave. Thus the assumption is made that all of the ferrocene centers on the support are oxidized at a single potential for multiferrocenyl assemblies.

Cyclic voltammograms of **1**−**3** are presented in Figure 8. A single oxidation−reduction was observed for both nanoparticles bearing the ferrocene ligand FcC{O}OCH_2CH_2−. The cathodic return wave is, in general, higher and thinner than the anodic forward wave, which has been attributed to some adsorption of the particles onto the surface of the electrode upon oxidation to the ferrocenium form.[23] This result is similar to that observed in cyclic voltammograms of $[Ag_7Br(SeCH_2CH_2O\{O\}CFc)_6(dppe)_3]$[8] and other clusters bearing the FcC{O}OCH_2CH_2− moiety, in addition to other reported nanoparticles bearing ferrocenyl termini.[14,23−28] The standard redox potential was estimated from the average values of the anodic and cathodic waves $[E_{1/2} = (E_{pa} + E_{pc})/2]$. Although the adsorption causes a small error, it was considered to be negligible. $E_{1/2}$ potentials of 700, 707, and 698 mV with peak separations ($E_{pa} - E_{pc}$) of 43, 33, and 32 mV were calculated for particles **1**−**3**, respectively, using a platinum working electrode. The I_{pa}/I_{pc} ratios were calculated to be 0.48 (**1**), 0.98 (**2**), and 0.96 (**3**). For an ideal system, the I_{pa}/I_{pc} should be equal to 1; lower values indicate adsorption to the electrode, as also suggested by the shape of the CV waves. Particle decomposition was not observed over time, as several repeated cycles showed no reduction in intensity or change in peak potential displaying the robustness of the particular clusters to oxidation. The stability of the particles in solution combined the simplicity of the reference CV (CV of nanoclusters: a single redox wave in the cyclic voltammogram) presented the opportunity for these materials to be explored as oxo-anion recognition materials.

Anion Recognition Studies. The selective detection of anions is a subject of intense research due to the biological and environmental role of these species.[24] Beer has shown various examples where these important anions can be recognized by mononuclear amidoferrocenes.[25] Further attempts to detect these anions have led to the use of nanomaterials, as they provide ideal nanoscale scaffolds for the conjugation of multiple copies of the redox receptor per molecule. Ferrocenyl groups have been attached to a wide variety of supports including endo receptors,[25,26] where the active site is contained within the molecule (crown ethers, cryptands, cyclophanes, etc.), and

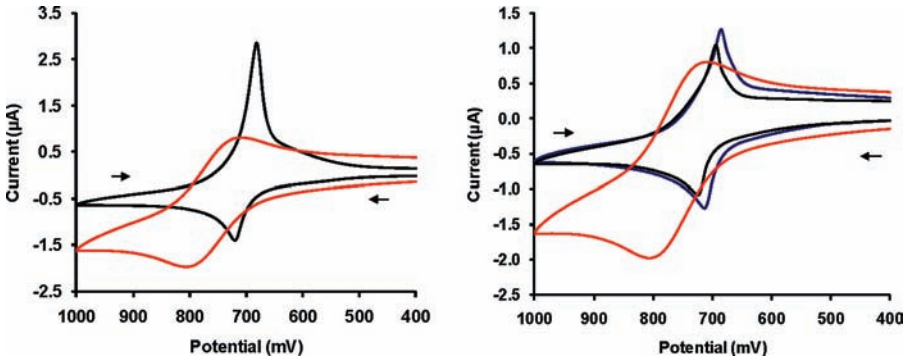

Figure 8. Cyclic voltammograms of (left) **1** (black) and (right) **2** (black) and **3** (blue) with $FcC\{O\}OCH_2CH_2Br$ (red) for comparison in CH_2Cl_2 with 0.1 M $[Bu_4N][PF_6]$ electrolyte at a scan rate of 100 mVs^{-1}. Arrows indicate the direction of the scan. Peak potentials are referenced to Ag/AgCl.

dendritic[27] and gold nanoparticle[23,28,29] exo receptors, where the active site(s) are on the surface of the molecules. Each functionalized material is accompanied by advantages and disadvantages. Dendrimers, for instance, display very good recognition of oxo-anions, with increased recognition as the dendrimer generations are increased. However, these materials can require complex syntheses. Gold nanoparticles, on the other hand, are very easily prepared with low size dispersity; however, they only show recognition as good as lower generation dendrimers. Functional groups are also an important aspect when developing these anion receptors, as a stronger interaction is often observed with oxo anions in conjunction with an amido, ureyl, or triazol group directly attached to the ferrocenyl redox moiety.[23,27,29] These functional groups interact with the anion in a supramolecular manner (ie. hydrogen bonding interactions) and can be responsible for the host−guest interaction that accounts for sensing. There are several factors allowing recognition by ferrocenyl functionalized materials: (i) the supramolecular interaction between the ferrocenyl side functional group and the anion, (ii) the ion-pairing interaction between the ferrocenium form and the anion, and (iii) the topological effect (the dense thiolate ligand shell around the particle forces the anion to penetrate into a narrow channel between the thiolate ligands). Although functional groups attached to the ferrocenyl moieties play an important role in anion recognition, electrostatic interactions have also been shown to sufficiently perturb the redox potential of the ferrocenyl group.[27g] No matter the type of interaction between the receptor and the anion, the ferrocenyl CV wave is generally shifted anodically in the case of a weak interaction or replaced by a new CV wave in the case of a strong interaction.[30]

The addition of $[Bu_4N][HSO_4]$ to a solution of the mononuclear complex $FcC\{O\}OCH_2CH_2Br$ in CH_2Cl_2 showed almost no change in the potential of the ferrocenyl CV waves upon the addition of 0.5 and 1 equivalent of $[Bu_4N][HSO_4]$, although a progressive decrease in the reduction wave was observed. Upon the addition of 1 equivalent of $[Bu_4N][HSO_4]$, a very weak shoulder is observed at slightly more negative potentials than the initial oxidation wave (738 mV vs 794 mV). The addition of increasing amounts (up to 6 equiv) of $[Bu_4N][HSO_4]$ provokes an increase in the current of this shoulder, resulting in a shift of the oxidation wave to more negative potentials (Figure 9). This latter aspect has been described by Astruc and co-workers as a result of the equilibrium between the ferrocenium ion pairing with the oxo anion, in this case, HSO_4^-, and with the anion of the supporting electrolyte, PF_6^- (Scheme 1). The ion pairing with HSO_4^- is favored over that with the PF_6^-. This is exhibited by

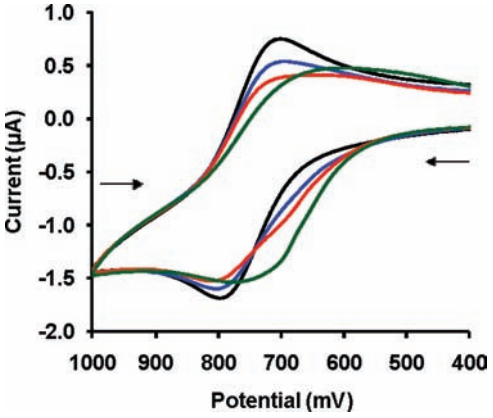

Figure 9. Cyclic voltammograms of $FcC\{O\}OCH_2CH_2Br$ in CH_2Cl_2 with 0.1 M $[Bu_4N][PF_6]$ electrolyte at a scan rate of 100 mVs^{-1} with the increasing addition of $[Bu_4N][HSO_4]$. Concentration of $[Bu_4N][HSO_4]$ added at 1 equiv, 1.5×10^{-3} M; $FcC\{O\}OCH_2CH_2Br$ only (black), 0.5 equiv $[Bu_4N][HSO_4]$ (blue), 1.0 equiv $[Bu_4N][HSO_4]$ (red), 6.0 equiv $[Bu_4N][HSO_4]$ (green). Arrows indicate the direction of scan. Peak potentials are referenced to Ag/AgCl.

Scheme 1. Formation of Ferrocenium Anion Complex upon Addition of Anion Salt[27g] (R = $C\{O\}OCH_2CH_2Br$)

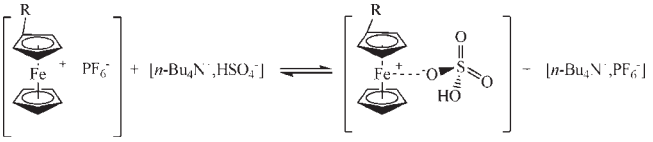

the fact that the supporting electrolyte is present at a concentration of 0.1 M, while the HSO_4^- even in excess to $FcC\{O\}OCH_2CH_2Br$ is only present in $\sim 10^{-4}$ M. Additionally, the fact that it requires such a large excess (6 equiv) to perturb the CV wave has been described to indicate that the alkyl branch sterically disfavors the contact ion pairing with the anion compared to that of the electrolyte (PF_6^-) due to a weakening of the supramolecular $Fe^+\cdots O^-$ bond, as only ~4 equiv of HSO_4^- was required to effectively perturb the CV of ferrocene.[27g]

The addition of $[Bu_4N][HSO_4]$ to a solution of **1** in CH_2Cl_2 provokes a shift of the reduction wave to more negative

dx.doi.org/10.1021/ic101717z |*Inorg. Chem.* 2011, 50, 3252–3261

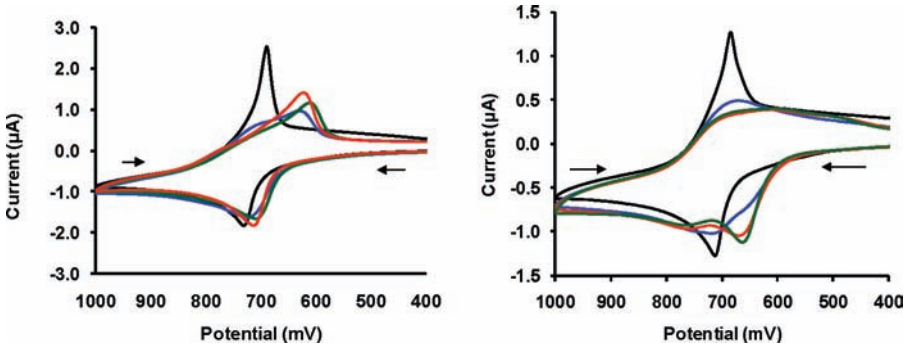

Figure 10. Cyclic voltammograms of **1** (left) and **3** (right) in CH_2Cl_2 with 0.1 M $[Bu_4N][PF_6]$ electrolyte at a scan rate of 100 mVs^{-1} with increasing addition of $[Bu_4N][HSO_4]$. Concentration of $[Bu_4N][HSO_4]$ added at 1 equiv 1.5×10^{-3} M: Particles only (black), 0.5 equiv $[Bu_4N][HSO_4]$ (blue), 1.0 equiv $[Bu_4N][HSO_4]$ (red), excess $[Bu_4N][HSO_4]$ (green). Arrows indicate the direction of the scan. Peak potentials are referenced to Ag/AgCl.

potentials (Figure 10, left). The addition of ~0.5 equiv of HSO_4^- has numerous marked effects on the cyclic voltammetry of **1**. A broadening of both the oxidation and reduction waves and a decrease in the current of the reduction wave are observed. Additionally, the CVs suggest that in the presence of the hydrogen sulfate anion there is no longer adsorption of the particles to the electrode surface. Adding another 0.5 equiv of HSO_4^- does not result in any further decrease in current, but it does cause a continued shift to more negative potentials of $E_{1/2}$ (710 → 656 mV). However, the shift observed for the oxidation wave is considerably less than that for the reduction wave. The addition of excess HSO_4^- (~ 6 equiv) results in a change in the reduction potential by 79 mV, with a smaller shift of 30 mV observed for the oxidation ($\Delta E_{1/2}$ of ~55 mV). The overall shift in potential is markedly weaker than that recorded for amidoferrocenyl dendrimers (9-Fc, 65 mV; 18-Fc, 130 mV); however, it is larger than that observed for some amidoferrocenylalkylthiolate (AFAT) modified gold nanoparticles (30 mV).[23] The fact that little change is observed in the oxidation wave upon the addition of HSO_4^- suggests that there is little interaction between the anion and the neutral form of the ferrocenyl ligands (E(particles) = 733 mV; E(particles + HSO_4^-) = 707 mV) . The ΔE ($E_{pa} - E_{pc}$) values typically illustrate the heterogeneous electron transfer rates and can be indicative of adsorption,[23] as shown for the free clusters. The larger ΔE value observed upon the interaction of **1** with the hydrogen sulfate anion (~ 100 mV) indicates that a somewhat slow electron transfer is taking place (ΔE > 59 mV). The cyclic voltammograms of **1** suggest a stronger interaction with HSO_4^- in the ferrocenium form than that observed for $FcC\{O\}OCH_2CH_2Br$, shown by the change in the CVs versus equivalents of HSO_4^- added. Upon the addition of ~0.5 equiv of HSO_4^-, a shift in the potential of the reduction wave from 688 mV to 629 mV is observed; however, a small shoulder corresponding to the initial reduction wave is still observed. The addition of a second ~0.5 equiv of HSO_4^- results in an increase of the new reduction wave (E_{pc} = 620 mV) and a complete disappearance of the initial reduction wave. The addition of excess HSO_4^- shows little change in the CV, suggesting that the equivalence point is reached at ~1−2 equiv of HSO_4^-/ferrocene branch. This value is considerably less than the 6 equiv required to perturb the CV of $FcC\{O\}OCH_2CH_2Br$, thus indicating the stronger interaction.

The addition of $[Bu_4N][HSO_4]$ to solutions of the larger particles **2** and **3** produces a very different effect than that observed for the smaller particles **1**. Figure 10 (right) summarizes cyclic voltammetry data for the addition of HSO_4^- to solutions of **3**. Particles **2** display almost (within 5 mV) identical CVs to those observed for **3** upon the addition of HSO_4^-; thus the data presented are representative of **2** and **3**. The addition of ~0.5 equiv of HSO_4^- leads to the appearance of an unresolved shoulder on the initial oxidation wave at a more negative potential. Additionally, a broadening and concomitant decrease in the current of both the oxidation and reduction waves is observed. As for **1**, in the presence of the HSO_4^- anion, the CVs suggests that there is no longer adsorption to the electrode surface. With increasing amounts of hydrogen sulfate (~ 1 equiv), the intensity of the new cathodically (shift to more negative potentials) shifted wave (E_{pa} = 665 mV) increases at the expense of that for the initial oxidation wave (E_{pa} = 715 mV). This is accompanied by a further loss of current of the reduction wave. The maximum shift of the potential from the initial oxidation wave to the new oxidation wave is approximately 53 mV, which was found to be the same for all of the larger clusters. Even after the addition of a large excess (~ 6 equiv) of HSO_4^-, the initial wave has not completely disappeared, although a larger peak separation (ΔE) is observed (96 mV) than for the particles in the absence of HSO_4^- (ΔE = 32 mV). The large peak separation is characteristic of a relatively slow heterogeneous electron transfer. The appearance of a new cathodically shifted wave indicates a stronger interaction of the HSO_4^- with the neutral form of the ferrocenyl ligands for the larger particles. A similar interaction has been described by Astruc and co-workers for gold nanoparticles functionalized with AFAT ligands containing an acetyl moiety bonded to the ferrocenes. These ligands offer the possibility of a stronger interaction with the HSO_4^- than that observed for AFAT,[23] although the shift in potential was considerably larger than that observed for the particles discussed here (130 mV versus 53 mV).

CONCLUSIONS

The use of the reagents $FcC\{O\}OCH_2CH_2ESiMe_3$ (E = S, Se) offers a general low temperature route for the incorporation of ferrocenyl units onto the surface of silver chalcogenide nanoclusters. These represent rare examples of such cluster materials prepared with a tailored redox active surface. The utility of $FcC\{O\}OCH_2CH_2ESiMe_3$ in combination with bis(trimethylsilyl)chalcogenide in reactions with silver acetate affords the ability to prepare monodisperse materials. In addition, it provides the ability to vary the size of the resulting particles by variation of the reaction stoichiometry. These materials display a simple cyclic voltammogram with a single oxidation and

dx.doi.org/10.1021/ic101717z |*Inorg. Chem.* 2011, 50, 3252–3261

reduction wave. The prepared particles effectively recognize HSO_4^-, as indicated by the shift in the reduction wave potential to more negative potentials upon the addition of $[Bu_4N][HSO_4]$.

■ ASSOCIATED CONTENT

Supporting Information. Thermogravimetric analysis results for **1** and **3** (Figures S1 and S2). Dynamic light scattering analysis results for **1**−**3** (Figures S3−S5). This material is available free of charge via the Internet at http://pubs.acs.org.

■ AUTHOR INFORMATION

Corresponding Author
*E-mail: corrigan@uwo.ca.

■ ACKNOWLEDGMENT

We thank the Natural Sciences and Engineering Research Council (NSERC) of Canada for financial support of this research and equipment funding. The Government of Ontario, The University of Western Ontario, and the Canada Foundation for Innovation are thanked for equipment funding. J.F.C. thanks the Center for Functional Nanostructures (Karlsruhe Institute of Technology) for support via a visiting professorship.

■ REFERENCES

(1) (a) Dehnen, S.; Eichhöfer, A.; Fenske, D. *Eur. J. Inorg. Chem.* **2002**, 279. (b) Deveson, A.; Dehnen, S.; Fenske, D. *J. Chem. Soc., Dalton Trans.* **1997**, 4491. (c) Dehnen, S.; Fenske, D. *Chem.—Eur. J.* **1996**, *2*, 1407. (d) Fenske, D.; Krautscheid, H. *Angew. Chem.* **1990**, *29*, 1452. (e) Eichhöfer, A.; Fenske, D. *J. Chem. Soc., Dalton Trans.* **1998**, 2969. (f) Zhu, N.; Fenske, D. *J. Chem. Soc., Dalton Trans.* **1999**, 1067. (g) Anson, C. E.; Eichhofer, A.; Issac, I.; Fenske, D.; Fuhr, O.; Sevillano, P.; Persau, C.; Stalke, D.; Zhang, J. *Angew. Chem., Int. Ed.* **2008**, *47*, 1326.

(2) (a) DeGroot, M. W.; Corrigan, J. F. *Comprehensive Coordination Chemistry II*; Fujita, M., Powell, A., Creutz, C., Eds; Pergamon: Oxford, England, 2004; Vol. 7, pp 57. (b) Fenske, D. *Clusters and Colloids, From Theory to Applications*; Schmid, G., Ed.; VCH: Weinheim, Germany, 1994; p 212. (c) Corrigan, J. F.; Fuhr, O.; Fenske, D. *Adv. Mater.* **2009**, *21*, 1867.(d) Dehnen, S.; Eichhöfer, A.; Corrigan, J. F.; Fuhr, O.; Fenske, D. *Nanoparticles: From Theory to Application*, 2nd ed.; Schmid, G., Ed.; Wiley-VCH: Weinheim, Germany, 2010; p 127.

(3) (a) Wallbank, A. I.; Corrigan, J. F. *Chem. Commun.* **2001**, 377. (b) Wallbank, A. I.; Corrigan, J. F. *J. Cluster Sci.* **2004**, *15*, 225. (c) Wallbank, A. I.; Borecki, A.; Taylor, N. J.; Corrigan, J. F. *Organometallics* **2005**, *24*, 788.

(4) Lebold, T. P.; Stringle, D. L. B.; Workentin, M. S.; Corrigan, J. F. *Chem. Commun.* **2003**, 1398.

(5) Ahmar, S.; MacDonald, D. G.; Vijayaratnam, N.; Battista, T. L.; Workentin, M. S.; Corrigan, J. F. *Angew. Chem., Int. Ed.* **2010**, *49*, 4422.

(6) (a) Nitschke, C.; Wallbank, A. I.; Fenske, D.; Corrigan, J. F. *J. Cluster Sci.* **2007**, *18*, 131. (b) Nitschke, C.; Fenske, D.; Corrigan, J. F. *Inorg. Chem.* **2006**, *45*, 9394.

(7) (a) So, J.-H.; Boudjouk, P. *Synthesis* **1989**, 306. (b) DeGroot, M. W.; Taylor, N. J.; Corrigan, J. F. *J. Mater. Chem.* **2004**, *14*, 654.

(8) MacDonald, D. G.; Eichhöfer, A.; Campana, C.; Corrigan, J. F. *Chem.—Eur. J.* **2011**.

(9) Ruiz Aranzaes, J.; Daniel, M.-C.; Astruc, D. *Can. J. Chem.* **2006**, *84*, 288.

(10) Dance, K. F. *Prog. Inorg. Chem.* **1994**, *41*, 637.

(11) Krautscheid, H.; Fenske, D.; Baum, G.; Semmelmann, M. *Angew. Chem., Int. Ed. Engl.* **1993**, *32*, 1303–1305.

(12) MacDonald, D. G.; Corrigan, J. F. *Dalton Trans.* **2008**, 5048.

(13) Hasan, M.; Bethell, D.; Brust, M. *J. Am. Chem. Soc.* **2002**, *124*, 1132.

(14) Wolfe, R. L.; Balasubramanian, R.; Tracy, J. B.; Murray, R. W. *Langmuir* **2007**, *23*, 2247.

(15) DeGroot, M. W.; Khadka, C.; Rösner, H.; Corrigan, J. F. *J. Cluster Sci.* **2006**, *17*, 97.

(16) Qian, J.; Jin, R. *Nano Lett.* **2009**, *9*, 4083.

(17) (a) Tang, K.; Xie, X.; Zhang, Y.; Zhao, X.; Jin, X. *Chem. Commun.* **2002**, 1024. (b) Chitzaz, S.; Fenske, D.; Fuhr, O. *Angew. Chem., Int. Ed.* **2006**, *45*, 8055. (c) Fenske, D.; Persay, C.; Dehnen, S.; Anson, C. *Angew. Chem., Int. Ed.* **2004**, *43*, 305.

(18) (a) Fenske, D.; Zhu, N.; Langetepe, T. *Angew. Chem., Int. Ed.* **1998**, *37*, 2640. (b) Fenske, D.; Anson, C. E.; Eichhöfer, A.; Fuhr, O.; Lngendoh, A.; Persau, C.; Richert, C. *Angew. Chem., Int. Ed.* **2005**, *44*, 5242.

(19) (a) Barr, T. H.; Watts, W. E. *J. Organomet. Chem.* **1968**, *15*, 177. (b) Nielson, D.; Farmer, M.; Eyring, H. *J. Phys. Chem.* **1976**, *80*, 717.

(20) Pileni, M. P.; Motte, L.; Billoudel, F.; Mahrt, J.; Willig., F. *Mater. Lett.* **1997**, *31*, 255.

(21) (a) Brühwiler, D.; Seifert, R.; Calzaferri, G. *J. Phys. Chem. B.* **1999**, *103*, 6397. (b) Brühwiler, D.; Leiggener, C.; Stephan, G.; Calzaferri, G. *J. Phys. Chem. B.* **2002**, *106*, 3770.

(22) (a) Flanagan, J. B.; Margel, S.; Bard, A. J.; Anson, F. C. *J. Am. Chem. Soc.* **1978**, *100*, 4248.(b) Bard, A. J.; Faulkner, R. L. *Electrochemical Methods*, 2nd ed.; Wiley: New York, 2001.

(23) (a) Labande, A.; Astruc, D. *Chem. Commun.* **2000**, 1007. (b) Lehn, J.-M. *Supramolecular Chemistry: Concepts and Perspectives*; VCH: Weinheim, 1995. (c) Labande, A.; Ruiz, J.; Astruc, D. *J. Am. Chem. Soc.* **2002**, *124*, 1782.

(24) Beer, P. D. *Angew. Chem., Int. Ed.* **2001**, *40*, 486.

(25) (a) Beer, P. D. *Adv. Inorg. Chem.* **1993**, *39*, 79. (b) Beer, P. D. *Chem. Commun.* **1996**, 689. (c) Beer, P. D. *Acc. Chem. Res.* **1998**, *31*, 71. (d) Beer, P. D.; Gale, P. A.; Chen, G. Z. *Adv. Phys. Org. Chem.* **1998**, *31*, 1. (e) Beer, P. D.; Hayes, E. J. *Coord. Chem. Rev.* **2003**, *240*, 167. (f) Beer, P. D.; Smith, D. K. *Prog. Inorg. Chem.* **2007**, 1.(g) Bayly, S. R.; Beer, P. D.; Chen, G. Z. In *Ferrocenes*; Petr, S., Ed.; Wiley: New York, 2008. (h) Bayly, S. R.; Beer, P. D. *Recognit. Anions* **2008**, *129*, 45.

(26) (a) Nlate, S.; Ruiz, J.; Sartor, V.; Navarro, R.; Blaiz, J.; Astruc, D. *Chem.—Eur. J.* **2000**, *6*, 2544. (b) Reynes, O.; Royal, G.; Chainet, E.; Moutet, J.-C.; Saint-Aman, E. *Electroanalysis* **2002**, *15*, 65. (c) Reynes, O; Gulon, T.; Moutet, J.-C.; Royal, G.; Saint-Aman, E. *J. Organomet. Chem.* **2002**, *656*, 116. (d) Reynes, O.; Moutet, J.-C.; Pecaut, J.; Royal, G.; Saint-Aman, E. *New J. Chem.* **2002**, *26*, 9. (e) Reynes, O.; Bucher, C.; Moutet, J. C.; Royal, G.; Saint-Aman, E.; Ungureanu, E. M. *J. Electroanal. Chem.* **2005**, *580*, 291. (f) Reynes, O.; Bucher, C.; Moutet, J.-C.; Royal, G.; Saint-Aman, E. *Inorg. Chim. Acta* **2008**, *361*, 1784.

(27) (a) Astruc, D.; Valério, C.; Fillaut, J.-L.; Ruiz, J.; Hamon, J.-R.; Varret, F. In *Supramolecular Magnetism*; Kahn, O., Ed.; Kluwer: Dordrecht, The Netherlands, 1996; NATO ASI Series, p 107. (b) Astruc, D.; Daniel, M.-C.; Ruiz, J. *Chem. Commun* **2004**, 2637. (c) Astruc, D.; Daniel, M.-C.; Ruiz, J. *Top. Organomet. Chem.* **2006**, *20*, 121. (d) Kaifer, A. E. *Eur. J. Inorg. Chem.* **2007**, 5015. (e) Astruc, D.; Ornelas, C.; Ruiz, J. J. *Inorg. Organomet. Polym. Mater.* **2008**, *18*, 1. (f) Astruc, D.; Ornelas, C.; Ruiz, J. *Acc. Chem. Res.* **2008**, *41*, 841. (g) Ornelas, C.; Ruiz, J.; Astruc, D. *Organometallics* **2009**, *28*, 4431.

(28) Stiles, R. L.; Balasubramanian, R.; Feldberg, S. W.; Murray, R. W. *J. Am. Chem. Soc.* **2008**, *130*, 1856.

(29) Daniel, M.-C.; Ruiz, J.; Nlate, S.; Blais, J.-C.; Astruc, D. *J. Am. Chem. Soc.* **2003**, *125*, 2617.

(30) Miller, S. R.; Gustowski, D. A.; Chen, Z-H; Gokel, G. W.; Echegoyen, L.; Kaifer, A. E. *Anal. Chem.* **1988**, *60*, 2021.

(31) (a) Valério, C.; Fillaut, J.-L.; Ruiz, J.; Guittard, J.; Blais, J.-C.; Astruc, D. *J. Am. Chem. Soc.* **1997**, *119*, 2588. (b) Valério, C.; Alonso, E.; Ruiz, J.; Blais, J.-C.; Astruc, D. *Angew. Chem., Int. Ed.* **1999**, *38*, 1747.